This is a pre-copyedited version of a contribution published in
Complex Networks and Their Applications VIII: Proceedings of the Eighth International Conference on Complex Networks and Their Applications (COMPLEX NETWORKS 2019)
Eds: Hocine Cherifi, Sabrina Gaito, José Fernendo Mendes, Esteban Moro Krumme and Luis Mateus Rocha.
Studies in Computational Intelligence Series, Springer.

Comparing Spectra of Graph Shift Operator Matrices

Johannes F. Lutzeyer and Andrew T. Walden

Imperial College London, London SW7 2AZ, UK,
jl7511@ic.ac.uk, a.walden@imperial.ac.uk

Abstract. Typically network structures are represented by one of three different graph shift operator matrices: the adjacency matrix and unnormalised and normalised Laplacian matrices. To enable a sensible comparison of their spectral (eigenvalue) properties, an affine transform is first applied to one of them, which preserves eigengaps. Bounds, which depend on the minimum and maximum degree of the network, are given on the resulting eigenvalue differences. The monotonicity of the bounds and the structure of networks are related. Bounds, which again depend on the minimum and maximum degree of the network, are also given for normalised eigengap differences, used in spectral clustering. Results are illustrated on the karate dataset and a stochastic block model. If the degree extreme difference is large, different choices of graph shift operator matrix may give rise to disparate inference drawn from network analysis; contrariwise, smaller degree extreme difference results in consistent inference.

Keywords: graph shift operator matrix, spectrum, clustering

1 Introduction

Networks can be represented in multiple ways via different graph shift operator matrices (GSOMs), typically by the adjacency matrix or normalised or unnormalised Laplacians. The degree d_i of the ith vertex is defined to be the sum of the weights of all edges connecting this vertex with others and the degree matrix D is defined to be the diagonal matrix $D = \text{diag}(d_1, \ldots, d_n)$. With the adjacency matrix denoted by A, the unnormalised graph Laplacian, L, is defined as $L = D - A$, and there are two commonly used normalised Laplacians defined as $L_{rw} = D^{-1}L$ and $L_{sym} = D^{-1/2}LD^{-1/2}$. The aim of this work is to compare the spectra (eigenvalues) of the GSOMs, A and L, and since the two normalised Laplacians are related by a similarity transform, so have identical eigenvalues, we choose to work with just one of these, namely L_{rw}.

The spectral properties of the GSOMs are utilised in many disciplines [4] for a broad range of different analysis methods, such as, the spectral clustering algorithm [16], graph wavelets [14], change point detection in dynamic networks [1] and the quantification of network similarity [7]. In particular, spectral clustering has had a big impact in the recent analysis of networks, with active research on

the theoretical guarantees which can be given for a clustering determined in this way ([11],[13]). The spectral properties of the different GSOMs are also starting to be leveraged in graph learning, as for example in [10]. It is the recommendation to use whichever GSOM works best in a particular analysis or learning task [12]. A framework under which the GSOM spectra can be compared and an improved understanding of the magnitude of the spectral differences of the GSOMs is of real use in informing such a decision.

In the remainder of the introduction we motivate the main ideas of the paper, which are the use of affine transformation to enable the comparison of the GSOM spectra, the affine transformation parameter choice and the bounds on the individual eigenvalue difference of the GSOMs. In Section 2 we provide bounds on the eigenvalue differences of the GSOMs for general graphs and visualise the effects of the affine transformation on the GSOM spectra corresponding to Zachary's karate social network. Then, in Section 3 we observe and explain the monotonicity of the eigenvalue bounds. In Section 4 we provide bounds on the difference of the normalised eigengaps (differences of successive eigenvalues) of the GSOMs and visualise them using a sample from a stochastic blockmodel. Section 5 highlights the impact of the GSOM choice on the inference drawn in graphical analysis by applying the spectral clustering algorithm using all three GSOMs to the karate network. In Section 6 we provide a summary and conclusions.

1.1 Motivation of the Affine Transformations

A direct comparison of the observed spectra is difficult. Primarily this is because for two of three comparisons to be made, the ordering of the eigenvalues is reversed; there is a rough correspondence of the *larger* end of the adjacency matrix spectrum to the the *smaller* end of the Laplacian spectra and vice versa for the other ends. Also, the supports of the three GSOM spectra are different [15, pp. 29, 64, 68]. (The upcoming Fig. 1 illustrates this.) For an insightful comparison it makes sense to relocate and scale the spectra (eigenvalues), $\mu_n \leq \cdots \leq \mu_1$, say, via an affine transformation $g(\mu) = c\mu + b$, where $c, b \in \mathbb{R}, c \neq 0$. Ordering is preserved for $c > 0$, i.e., $g(\mu_1) \geq g(\mu_2)$ and reversed for $c < 0$, i.e., $g(\mu_1) \leq g(\mu_2)$. Eigengaps, relative to the spectral support, are preserved. Assume the domain of g is equal to the interval $[x_1, x_2]$, so g's image is equal to $[g(x_1), g(x_2)]$. Then normalised eigengaps are preserved:

$$\frac{\mu_1 - \mu_2}{x_2 - x_1} = \frac{c\,(\mu_1 - \mu_2) + b - b}{c\,(x_2 - x_1) + b - b} = \frac{g(\mu_1) - g(\mu_2)}{g(x_2) - g(x_1)}. \tag{1}$$

In the spectral clustering algorithms, eigengaps are used to determine the number of clusters in the network, while the eigenvalue ordering is used to identify which eigenvectors to consider [16]. Therefore, when comparing the impact of the choice of GSOMs on graphical analysis, we need to preserve or reverse eigenvalue ordering and preserve relative eigengap size.

1.2 Motivation of the Parameter Choice

All three GSOMs are related through the degree matrix D. Denote the degree extremes by $d_{\min}$ and $d_{\max}$. For d-regular graphs, where $d_{\max} = d_{\min} = d$, the GSOMs are already exactly related by affine transformations and hence their eigenvalues are related by the same affine transformations. For general (non-d-regular graphs) we shall make parameter choices for the affine transformations such that eigenvalue differences, after affine transformation, can be bounded above in terms of the elements of D. These general parameter choices agree with the natural existing transformation parameters for d-regular graphs.

1.3 Motivation for Calculating a Bound on the Eigenvalue Differences

The motivation for bounding the eigenvalue difference is twofold. On the one hand, the structure of the bound and its dependency on network parameters allow us to infer for which graphs we are able to see larger differences in the GSOM spectra. On the other hand, the bounds allow us to add a sensible scale to observed eigenvalues; the bound represents the theoretically maximal distance the eigenvalues and eigengaps can differ by and therefore we are able to compare observed differences to the maximal possible differences.

2 GSOM Eigenvalue Differences

2.1 Transforms and Bounds

Theorem 1. *Consider a graph G with degree extremes $d_{\min}$ and $d_{\max}$. Let the eigenvalues of the corresponding adjacency matrix A and unnormalised Laplacian matrix L be denoted by $\mu_n \leq \cdots \leq \mu_1$ and $\lambda_1 \leq \cdots \leq \lambda_n$, respectively. Then, there exists a transformation $f_1(\mu_i) = c_1\mu_i + b_1$, where $c_1 = -1$ and $b_1 = (d_{\max} + d_{\min})/2$, such that for all $i \in \{1, \cdots, n\}$,*

$$|f_1(\mu_i) - \lambda_i| \leq \frac{d_{\max} - d_{\min}}{2} \stackrel{\text{def}}{=} e(A, L). \tag{2}$$

For d-regular graphs, (2) gives $e(A, L) = 0$, so that $f_1(\mu_i) = \lambda_i = c_1\mu_i + b_1 = d - \mu_i$, i.e., the eigenvalues are related by the required exact relation, as claimed in Section 1.2.

For general graphs, using (2), we can establish a rough correspondence, to within an affine transformation, between the eigenvalues of the adjacency matrix, A, and the unnormalised graph Laplacian, L, if the extremes of the degree sequence $d_{\max}$ and $d_{\min}$ are reasonably close.

Theorem 2. *Consider a graph G with degree extremes $d_{\min} > 0$ and $d_{\max}$. Let the eigenvalues of L and L_{rw} be denoted by $\lambda_1 \leq \cdots \leq \lambda_n$ and $\eta_1 \leq \cdots \leq \eta_n$, respectively. Then, there exists a transformation $f_2(\lambda_i) = c_2\lambda_i + b_2$, where $c_2 = 2/(d_{\max} + d_{\min})$ and $b_2 = 0$, such that for all $i \in \{1, \cdots, n\}$,*

$$|f_2(\lambda_i) - \eta_i| \leq 2\,\frac{d_{\max} - d_{\min}}{d_{\max} + d_{\min}} \stackrel{\text{def}}{=} e\left(L, L_{rw}\right). \tag{3}$$

Asymptotically, as $d_{\max} \to \infty$ with fixed $d_{\min} > 0$, the bound $e\,(L, L_{rw})$ tends to 2. The restricted range of $d_{\min}$ is due to D^{-1}, the normalised Laplacian and consequently the bound $e(L, L_{rw})$ not being defined for $d_{\min} = 0$. For d-regular graphs, where $d_{\max} = d_{\min} = d$, the bound equals zero. Hence, the spectra of $f_2(L)$ and L_{rw} are equal and $\eta_i = c_2\lambda_i = \lambda_i/d$, i.e., the eigenvalues are related by the required exact relation. Overall, the behaviour of this bound is similar to $e(A, L)$. The smaller the difference of the degree sequence extremes $d_{\max}$ and $d_{\min}$, the closer the spectra of L and L_{rw} are related, signified by a smaller bound on the eigenvalue differences.

Theorem 3. *Consider a graph G with degree extremes $d_{\min} > 0$ and $d_{\max}$. Let the eigenvalues of A and L_{rw} be denoted by $\mu_n \leq \cdots \leq \mu_1$ and $\eta_1 \leq \cdots \leq \eta_n$, respectively. Then, there exists a transformation $f_3(\mu_i) = c_3\mu_i + b_3$, where $c_3 = -2/(d_{\max} + d_{\min})$ and $b_3 = 1$, such that for all $i \in \{1, \cdots, n\}$,*

$$|f_3(\mu_i) - \eta_i| \leq \frac{d_{\max} - d_{\min}}{d_{\max} + d_{\min}} \stackrel{\text{def}}{=} e\,(A, L_{rw})\,. \tag{4}$$

For d-regular graphs, $e\,(A, L_{rw})$ equals zero and hence the spectra of $f_3(A)$ and L_{rw} are equal and $\eta_i = 1 + c_3\mu_i = 1 - (\mu_i/d)$, i.e., the spectra of L_{rw} and A are related by the required exact relation. For general graphs, $e(A, L_{rw})$ is small for small degree extreme differences and hence the spectra of the two GSOMs exhibit smaller maximal differences, as was the case for $e(A, L)$ and $e(L, L_{rw})$.

The proofs of Theorems 1, 2 and 3 directly follow from inequality (4.3) in [2, p. 46], choosing parameters c_1, b_2 and b_3 as given in the theorem statements to make the problem analytically solvable and by then analytically minimising the two norm. More detailed proofs of the theorems are available from the authors upon request.

2.2 Karate Dataset Example

The karate dataset [3] dates back to [18]. We work with a square matrix with 34 entries, '`ZACHE`,' which is the adjacency matrix of a social network describing presence of interaction in a university karate club. This data set is popular as it naturally lends itself to clustering [5, 8, 9].

The untransformed and transformed eigenvalues of the GSOMs A, L and L_{rw} of Zachary's karate dataset are shown in Fig. 1. From Figs. 1(a), (b) and (c) not much can be said about how the spectra compare. From Figs. 1(d), (e) and (f) it can be observed that each pair of spectra of the karate dataset cover a similar range after transformation and that clearly the spectra of A and L_{rw} are the most similar of the three. It can also be seen that the largest eigengaps occur at opposing ends of the spectra when comparing A and L_{rw} with L. This observation is only possible from the plots including the transforms, i.e., Figs. 1(d), (e) and (f). Clearly, the eigenvalue spectra become more comparable through utilising the proposed transformations.

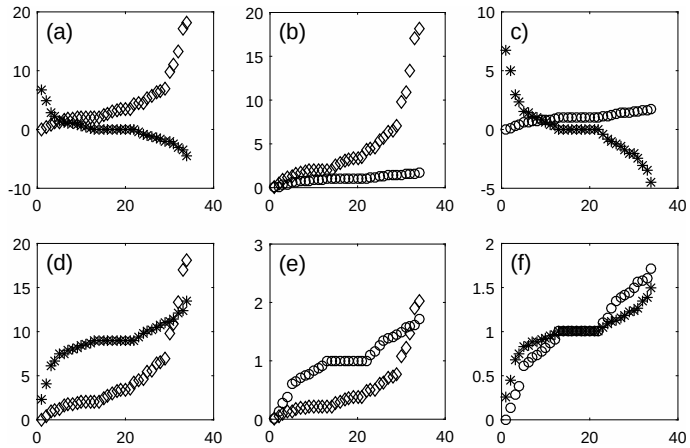

Fig. 1. Transformation results for Zachary's karate dataset. First row: (a) eigenvalues μ of A (stars) and λ of L (diamonds); (b) eigenvalues λ of L and η of L_{rw} (circles); (c) eigenvalues μ of A and η of L_{rw}. Second row: the first of the two eigenvalue spectra are transformed by their respective transformations f_1, f_2 and f_3.

Remark 1. [19, p. 32] shows that vertices with identical neighbourhoods generate eigenvalues equal to 0 and 1 in the adjacency and normalised Laplacian spectrum, respectively. Interestingly, we spot several such vertices in the karate network, which will be shown in Fig. 4, and several corresponding eigenvalues equal to 0 and 1 in Fig. 1(c). It is very nice to see that the equivalence of these eigenvalues is highlighted by our transformation mapping them exactly onto each other in Fig. 1(f). $\triangleleft$

In Fig. 2, we display a proof of concept of our bounds. The eigenvalue bounds are centred around the average value of each eigenvalue pair in order to highlight the maximal difference achievable by each individual eigenvalue pair under comparison. For the karate dataset the bound values $(e(A, L), e(L, L_{rw}), e(A, L_{rw}))$ are equal to $(8.00, 1.78, 0.89)$. The particular bounds displayed here are valid for all graphs with $d_{\min} = 1$ and $d_{\max} = 17$, i.e., all graphs in $\mathcal{C}_{1,17}$, where $\mathcal{C}_{j,k}$ is the class of graphs with $d_{\min} = j$ and $d_{\max} = k$. The bounds being almost attained in plot (a), and not attained in plots (b) and (c), is more a consequence of the structure of the graph given by the karate data set than tightness and quality of the bounds. Since the three bounds $e(A, L)$, $e(L, L_{rw})$ and $e(A, L_{rw})$ apply to entire classes $\mathcal{C}_{j,k}$ at a time, we can only achieve tightness on these classes — bounds being attained for some elements in $\mathcal{C}_{j,k}$ — and not on each individual element of them.

So for our particular social network, the karate dataset, firstly the bound being almost attained in plot (a) tells us that the spectra of A and L deviate almost as much as theoretically possible for a graph in $\mathcal{C}_{1,17}$. Secondly, from plot (c) we see that the spectra of A and L_{rw} are rather similar for the karate data

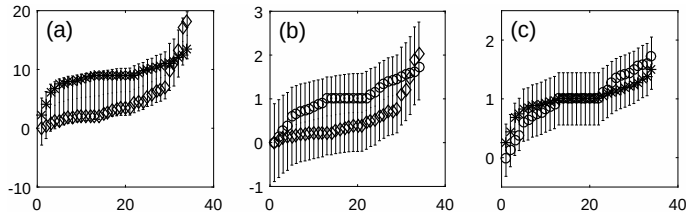

Fig. 2. Eigenvalue bounds on the karate eigenvalues. In plot (a) we display the bound $e(A, L)$ via the intervals together with the transformed eigenvalues of the adjacency matrix $f_1(\mu)$ (stars) and the eigenvalues of the Laplacian λ (diamonds). (b) the bound $e(L, L_{rw})$ is displayed via the intervals, the diamonds correspond to the transformed Laplacian eigenvalues $f_2(\lambda)$ and the circles are the eigenvalues of the normalised graph Laplacian η. (c) the bound $e(A, L_{rw})$ is displayed via the intervals, the stars correspond to the transformed adjacency eigenvalues $f_3(\mu)$ and the circles are the normalised Laplacian eigenvalues η.

Table 1. Comparing bounds on eigenvalue differences of A, L and L_{rw}. The bound values are displayed as $(e\,(A, L)\,, e\,(L, L_{rw})\,, e\,(A, L_{rw}))$.

	$d_{\min}$				
	0	1	2	3	4
1	(0.5, ·, ·)	(0, 0, 0)	*	*	*
2	(1, ·, ·)	(0.5, 0.67, 0.33)	(0, 0, 0)	*	*
3	(1.5, ·, ·)	(1, 1, 0.5)	(0.5, 0.4, 0.2)	(0, 0, 0)	*
$d_{\max}$ 4	(2, ·, ·)	(1.5, 1.2, 0.6)	(1, 0.67, 0.33)	(0.5, 0.29, 0.14)	(0, 0, 0)
5	(2.5, ·, ·)	(2, 1.33, 0.67)	(1.5, 0.86, 0.43)	(1, 0.5, 0.25)	(0.5, 0.22,0.11)
6	(3, ·, ·)	(2.5, 1.43, 0.71)	(2, 1, 0.5)	(1.5, 0.67, 0.33)	(1, 0.4, 0.2)

set and could theoretically deviate significantly more for a different graph in $\mathcal{C}_{1,17}$ having degree extreme difference 16. The bounds give us insight into how particular GSOM spectra behave for the karate dataset.

3 Relating the Spectral Bounds

We display some sample bound values in Table 1. The first column of Table 1 only contains values of $e(A, L)$ as for $d_{\min} = 0$ the normalised Laplacian and hence $e(L, L_{rw})$ and $e(A, L_{rw})$ are not well-defined. In practice this is of little consequence since disconnected nodes are commonly removed from the dataset as a preprocessing step. On the diagonal of Table 1, where $d_{\max} = d_{\min}$, i.e., for the d-regular graphs, we find $e\,(A, L) = e\,(L, L_{rw}) = e\,(A, L_{rw}) = 0$ due to the direct spectral relation of the GSOMs.

Remark 2. It is interesting to note, that since the spectral support of neither A, nor L, is bounded, the bound on their eigenvalue difference is also not bounded above. (This explains the large values in Fig. 2(a)). This does not apply to the other two bounds as we have $e\left(L, L_{rw}\right) \leq 2$ and $e\left(A, L_{rw}\right) \leq 1$. $\triangleleft$

Before discussing the structure of Table 1, we define connected components in a graph.

Definition 1. *A* path *on a graph G is an ordered list of unique vertices such that consecutive vertices are connected by an edge. A vertex set S_k is called a* connected component *if there exists a path between any two vertices $v_i, v_j \in S_k$ and there exists no path from any $v_i \in S_k$ to any $v_j \notin S_k$.* $\triangleleft$

Since all graphs in $\mathcal{C}_{j+1,k}$ can be extended to lie in $\mathcal{C}_{j,k}$ by adding one or more connected components, all spectra of graphs in $\mathcal{C}_{j+1,k}$ are subsets of spectra of graphs in $\mathcal{C}_{j,k}$ (the GSOM spectrum of a graph is the union of the spectra of its connected components [6, p. 7]). Therefore, the support of the spectra of graphs in $\mathcal{C}_{j,k}$ must be larger or equal to the support of spectra of graphs in $\mathcal{C}_{j+1,k}$. Hence, we expect the spectral bounds, $e(\cdot,\cdot)$, we derived to be decreasing or constant with increasing $d_{\min}$ and constant $d_{\max}$. This phenomenon can be observed in Table 1 when traversing each *row*.

In similar fashion, any graph in $\mathcal{C}_{j,k}$, can be extended to be a graph in $\mathcal{C}_{j,k+1}$, by adding a connected component with all vertex degrees greater or equal to j and smaller or equal than $k+1$ with at least one node attaining degree $k+1$. Then spectra of graphs in $\mathcal{C}_{j,k}$ are subsets of spectra of graphs $\mathcal{C}_{j,k+1}$ and therefore the spectral support and hence the spectral bounds on $\mathcal{C}_{j,k+1}$ have to be greater or equal than the respective quantities for $\mathcal{C}_{j,k}$. So, any of the spectral bounds, $e(\cdot,\cdot)$, will be increasing or constant with increasing $d_{\max}$ and constant $d_{\min}$, as seen in the *columns* of Table 1.

4 GSOM Normalised Eigengap Differences

Here we derive bounds on the normalised eigengap differences, where each eigengap is normalised by the spectral support of its corresponding GSOM.

Let $\mathcal{M}_i$ denote the ith eigengap of A, $\mathcal{M}_i = \mu_i - \mu_{i+1}$, $\mathcal{L}_i$ denote the ith eigengap of L, $\mathcal{L}_i = \lambda_{i+1} - \lambda_i$ and $\mathcal{N}_i$ denote the ith eigengap of L_{rw}, $\mathcal{N}_i = \eta_{i+1} - \eta_i$, for $i \in \{1, 2, \ldots, n-1\}$. The spectral supports of A, L and L_{rw} are equal to $[-d_{\max}, d_{\max}]$, $[0, 2d_{\max}]$ and $[0, 2]$, respectively [15, pp. 29, 64, 68], so the lengths of the supports are $\ell(\mu) = \ell(\lambda) = 2d_{\max}$ and $\ell(\eta) = 2$.

From (1) we see that the normalisation of transformed eigengaps by the transformed spectral support is equal to the normalisation of the untransformed eigengaps by the untransformed spectral support. We will therefore start our analysis by considering the untransformed normalised eigengaps. Eigengap normalisation by the spectral support of the corresponding GSOM is crucial to be able to make a meaningful comparison of eigengap magnitudes.

Theorem 4. *Bounds on the normalised eigengap difference of the GSOMs are given by*

$$\left|\frac{\mathcal{M}_i}{2d_{\max}} - \frac{\mathcal{L}_i}{2d_{\max}}\right| \leq \frac{d_{\max} - d_{\min}}{2d_{\max}} \stackrel{\text{def}}{=} g(A, L);$$
$$\left|\frac{\mathcal{L}_i}{2d_{\max}} - \frac{\mathcal{N}_i}{2}\right| \leq 2\frac{d_{\max} - d_{\min}}{d_{\max}} \stackrel{\text{def}}{=} g(L, L_{rw});$$
$$\left|\frac{\mathcal{M}_i}{2d_{\max}} - \frac{\mathcal{N}_i}{2}\right| \leq \frac{d_{\max} - d_{\min}}{d_{\max}} \stackrel{\text{def}}{=} g(A, L_{rw}).$$

The proofs of the three inequalities in Theorem 4 directly follow by applying the triangle inequality and then varying the proofs of Theorems 1, 2 and 3 slightly to accommodate the normalisation of the spectra as transformation parameters. More detailed proofs of the theorems are available from the authors upon request.

4.1 Stochastic Blockmodel Example

We see that the eigengaps of the GSOMs are different, giving further evidence that the graphical structure captured in the different spectra differs significantly and possibly in a structured manner. Furthermore, we have been able to use our bounds to put the magnitude of the observed eigengaps into the broader perspective of all graphs with corresponding degree extremes.

The stochastic blockmodel, which is widely used in the networks literature [9, 11], allows us to encode a block structure in a random graph via different probabilities of edges within and between node-blocks. Our definition and parametrisation is adapted from [11].

Definition 2. *Consider a graph with node set $\{v_1, \ldots, v_n\}$. Split this node set into K disjoint blocks denoted $\mathcal{B}_1, \ldots, \mathcal{B}_K$. We encode block membership of the nodes via a membership matrix $M \in \{0,1\}^{n \times K}$, where $M_{i,j} = 1$ if $v_i \in \mathcal{B}_j$ and $M_{ij} = 0$ otherwise. Finally, we fix the probability of edges between blocks to be constant and collect these probabilities in a probability matrix $P \in [0,1]^{K \times K}$, i.e., for nodes $v_i \in \mathcal{B}_l$ and $v_j \in \mathcal{B}_m$ the probability of an edge between v_i and v_j is equal to $P_{l,m}$.* $\triangleleft$

Hence, the parameters of the stochastic blockmodel are $M \in \{0,1\}^{n \times K}$ and $P \in [0,1]^{K \times K}$, where the number of nodes $n \in \mathbb{N}$ and the number of clusters $K \in \mathbb{N}$ are implicitly defined via the dimensions of M. We simulate graphs from this model by fixing these parameters and then sampling edges from Bernoulli trials. The Bernoulli parameter of the trial corresponding to the edge connecting v_i to v_j is given by the $(i,j)^{\text{th}}$-entry of the matrix MPM^T.

Fig. 3 contains eigengaps corresponding to the three GSOMs of a graph arising as a realisation of a stochastic blockmodel with parameters $n = 600$; $K = 6$; $M_{1,1} = \ldots = M_{100,1} = M_{101,2} = \ldots = M_{200,2} = M_{201,3} = \ldots = M_{300,3} = M_{301,4} = \ldots = M_{400,4} = M_{501,6} = \ldots = M_{600,6} = 1$ and all other

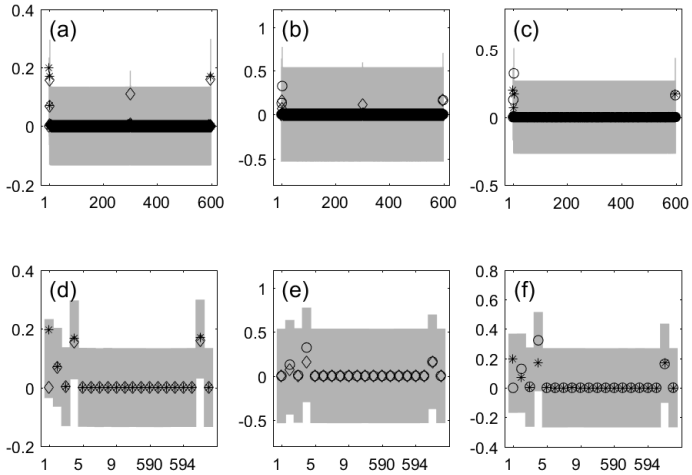

Fig. 3. Plots (a), (b) and (c) display all normalised eigengaps and plots (d), (e) and (f) display the first and last 10 normalised eigengaps of a graph sampled from a stochastic blockmodel. The stars correspond to eigengaps of A normalised by the spectral support of A, the diamonds display the corresponding quantity for L and the circles represent the corresponding quantity for L_{rw}. The filled light grey area delineates the three bounds, where $g(A, L)$ is displayed in plots (a) and (d), $g(L, L_{rw})$ is shown in plots (b) and (e) and $g(A, L_{rw})$ is displayed in plots (c) and (f).

entries of M equal 0;

$$P = \begin{pmatrix} 0.9 & 0.1 & 0.1 & 0 & 0 & 0 \\ 0.1 & 0.9 & 0.1 & 0 & 0 & 0 \\ 0.1 & 0.1 & 0.9 & 0 & 0 & 0 \\ 0 & 0 & 0 & 0.1 & 0.9 & 0.9 \\ 0 & 0 & 0 & 0.9 & 0.1 & 0.9 \\ 0 & 0 & 0 & 0.9 & 0.9 & 0.1 \end{pmatrix}.$$

Hence, we have a network of 6 blocks with 100 nodes per block. From observation of P, we recognise that all realisations from this model consist of at least *two connected components* since the probability of an edge between blocks $\{\mathcal{B}_1, \mathcal{B}_2, \mathcal{B}_3\}$ and $\{\mathcal{B}_4, \mathcal{B}_5, \mathcal{B}_6\}$ is equal to 0.

In order to gain more insight into the block structure of this stochastic blockmodel we consider different definitions of clusters or blocks. [13] describe so called '*heterophilic*' clusters, which they recover from the eigenvectors corresponding to the extreme negative eigenvalues of the normalised Laplacian. These heterophilic clusters have fewer connections within than between clusters and are exemplified by romantic relationship graphs where the genders are the two biggest clusters identifiable. Our blockmodel includes such heterophilic blocks in $\{\mathcal{B}_4, \mathcal{B}_5, \mathcal{B}_6\}$. While blocks $\{\mathcal{B}_1, \mathcal{B}_2, \mathcal{B}_3\}$ form clusters in the more traditional sense with more edges within rather than between blocks, which will be referred to as '*homophilic*' cluster structure for the remainder of this analysis.

In the analysis of Fig. 3, we interpret large eigengaps in the context of spectral clustering. Firstly, large eigengaps are understood to indicate the number

of clusters discovered by the different GSOMs, i.e., a large K^{th} eigengap is understood to indicate a clustering into K communities [16, p. 410]. Secondly, the size of the eigengap is understood to represent relative strength of evidence for a certain clustering [16, p. 407].

In Fig. 3 we find that all three spectra have a non-zero normalised eigengap with indices 2, 4 and 598. In addition, A has a large first normalised eigengap and L a large 301st normalised eigengap; with the exception of these two large eigengaps, in the context of the spectral clustering algorithms the eigengaps suggest searching for similar numbers of clusters.

From [16, pp. 397–8] we know that the nonzero second eigengap of the Laplacians in Fig. 3 encodes the separation of the network into two connected components. It is interesting to see that all GSOM spectra contain stronger evidence for the block structure within the two connected components of the stochastic blockmodel, encoded by the large 4th and 598th normalised eigengaps, than the clustering into the two connected components themselves, encoded by the large 2nd normalised eigengaps. It is especially interesting that for A and L the 4th and 598th normalised eigengaps are approximately equal, while for L_{rw} the 4th normalised eigengap is almost twice as large as the 598th normalised eigengap. Both components have symmetric parameters and therefore it is very interesting that the eigengaps in L_{rw} suggest stronger evidence for the homophilic cluster structure encoded by the 4th eigengap rather than the heterophilic cluster structure encoded by the 598th eigengap. A much larger simulation of stochastic blockmodels with varying parameters, which is beyond the scope of this work, could establish whether L_{rw} does indeed have a structured preference for homophilic over heterophilic blocks.

5 Application to Spectral Clustering

To illustrate the impact of the GSOM choice, we display the spectral clustering according to the first two eigenvectors of each of the three GSOMs corresponding to the karate data set. The choice of GSOM has a significant impact on the clustering outcome. We use the simplest form of spectral clustering by running the k-means algorithm on the rows of the first k eigenvectors of the different GSOMs [16, p. 399].

Since for the karate dataset, we have a reasonably large degree extreme difference, $d_{\max} - d_{\min} = 16$, we expect to see deviating results in the spectral clustering according to the different GSOMs.

At first sight, all clusterings displayed in Fig. 4 seem sensible. The clustering according to the adjacency matrix extends the cluster marked with the unfilled, square nodes by one node, karate club member 3, in comparison to the clustering according to the normalised Laplacian. In contrast, the unnormalised Laplacian detects 5 nodes less (karate club members 2, 4, 8, 14 and 20) in the cluster marked by the unfilled square nodes, than does the normalised Laplacian.

We find the clustering according to the adjacency matrix A to agree with the ground truth clustering into social factions within the karate club as recorded by

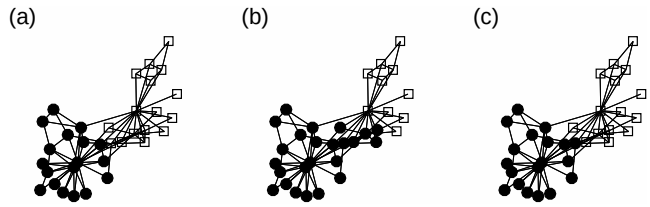

Fig. 4. Spectral clustering of the karate network according to the first two eigenvectors of the adjacency matrix A in (a), the unnormalised Laplacian L in (b) and the normalised Laplacian L_{rw} in (c).

[18]. The normalised Laplacians misplace one out of 34 nodes, which is known to be difficult to cluster correctly in the literature [8]. The unnormalised Laplacian however, misplaces 6 nodes, only one of which is known to us to be commonly misclustered. Hence, the unnormalised Laplacian clustering is clearly outperformed by the other two GSOMs when using the first two eigenvectors to find two communities in the karate data set. In [17] the conditions under which spectral clustering using the unnormalised Laplacian converges are shown to be more restrictive than the conditions under which spectral clustering according to the normalised Laplacian converges. [17] hence advocate using the normalised Laplacian for spectral clustering over the unnormalised Laplacian. Our clustering results agree with this recommendation.

Remark 3. GSOM choice can clearly impact cluster inference results via spectral clustering. We suggest considering degree extreme difference as a parameter in graphical signal processing to infer potential impact of the choice of GSOM. $\triangleleft$

6 Summary and Conclusions

We have compared the spectra of the GSOMs: the adjacency matrix A, the unnormalised graph Laplacian L and the normalised graph Laplacian L_{rw} and found differences in the spectra corresponding to general graphs. For all three pairs of GSOMs the degree extreme difference, $d_{\max} - d_{\min}$, was found to linearly upper bound both the spectral differences, when transforming one of the two spectra by an affine transformation, and the normalised eigengap differences. We explained the monotonicity found in the eigenvalue bounds by partitioning the class of graphs according to their degree extremes and considering the addition/deletion of connected components to/from the graph. Our bounds were illustrated on Zachary's karate network and on a network sampled from a stochastic blockmodel with homophilic and heterophilic cluster structures. *We find that if the degree extreme difference is large, different choices of GSOMs may give rise to disparate inference drawn from network analysis; smaller degree extreme differences will result in consistent inference, whatever the choice of GSOM.* The significant differences in inference drawn from graphical analysis

using the different GSOMs were illustrated via the spectral clustering algorithm applied to Zachary's karate network.

References

1. Aleardi, L.C., Salihoglu, S., Singh, G., Ovsjanikov, M.: Spectral Measures of Distortion for Change Detection in Dynamic Graphs In: Aiello, L.M., Cherifi, C., Cherifi, H., Lambiotte, R., Lió, P., Rocha, L.M. (eds) Complex Networks and Their Applications VII, pp. 54–66, Springer (2019). doi:10.1007/978-3-030-05414-4_5
2. Bai, Z., Demmel, J., Dongarra, J., Ruhe, A., van der Vorst, H.: Templates for the solution of algebraic eigenvalue problems: a practical guide. SIAM (2000).
3. Batagelj, V., Mrvar, A.: Pajek datasets, http://vlado.fmf.uni-lj.si/pub/networks/data/ (2006). Accessed: 2016-11-23
4. Cvetkovic, D., Gutman, I.: Applications of graph spectra: An introduction to the literature. Zbornik radova, vol. 14, pp. 9–34 (2011).
5. Chen, P.Y., Hero,A.O.: Deep community detection. IEEE Trans. Signal Process. vol. 63, pp. 5706–5719 (2015). doi:10.1109/TSP.2015.2458782
6. Chung, F.R.K.: Spectral graph theory. American Mathematical Soc. (1997).
7. Crawford, B., Gera, R., House, J.,Knuth, T., Miller, R.: Graph Structure Similarity using Spectral Graph Theory In: Cherifi, H., Gaito, S., Quattrociocchi, W.,Sala, A. (eds) Complex Networks & Their Applications V, pp. 209–221, Springer (2017). doi:10.1007/978-3-319-50901-3_17
8. Fortunato, S.: Community detection in graphs. Phys. Rep., vol. 486, pp. 75–174 (2010). doi:10.1016/j.physrep.2009.11.002
9. Karrer, B., Newman, M.E.J.: Stochastic blockmodels and community structure in networks. Phys. Rev. E, vol. 83, pp. 016107 (2011). doi:10.1103/PhysRevE.83.016107
10. Kumar, S., Ying, J., Cardoso, J.V. de M., Palomar, D.P.: A Unified Framework for Structured Graph Learning via Spectral Constraints. arXiv:1904.09792 [stat.ML] (2019).
11. Lei, J., Rinaldo, A.: Consistency of spectral clustering in stochastic block models. Ann. Stat., vol. 43, pp. 215–237 (2015). doi:10.1214/14-AOS1274
12. Ortega, A., Frossard, P., Kovacevic, J., Moura, J.M.F., Vandergheynst, P.: Graph Signal Processing: Overview, Challenges, and Applications. Proc. IEEE, vol. 106, pp. 808–828 (2018). doi:10.1109/JPROC.2018.2820126
13. Rohe, K., Chatterjee, S., Yu, B.: Spectral clustering and the high-dimensional stochastic blockmodel. Ann. Stat., vol. 39, pp. 1878–1915 (2011). doi:10.1214/11-AOS887
14. Tremblay, N., Borgnat, P.: Graph wavelets for multiscale community mining. IEEE Signal Process. Mag., vol. 62, pp. 5227–5239 (2014). doi:10.1109/TSP.2014.2345355
15. van Mieghem, P.: Graph Spectra for Complex Networks. Cambridge University Press, Cambridge U.K. (2011).
16. von Luxburg, U.: A tutorial on spectral clustering. Stat. Comput., vol. 17, pp. 395–416 (2007). doi:10.1109/TSP.2015.2458782
17. von Luxburg, U., Belkin, M., Bousquet, O.: Consistency of spectral clustering. Ann. Stat., vol. 36, pp. 555–586 (2008). doi:10.1214/009053607000000640
18. Zachary, W.W.: An information flow model for conflict and fission in small groups. J. Anthropol. Res., vol. 33, pp. 452–473 (1977). doi:10.1086/jar.33.4.3629752
19. Zumstein, P., Comparison of Spectral Methods Through the Adjacency Matrix and the Laplacian of a Graph. PhD thesis, ETH Zürich (2005).